Image Restoration from a Sequence of Random Masks

CONFERENCE PAPER *in* PROCEEDINGS OF SPIE - THE INTERNATIONAL SOCIETY FOR OPTICAL ENGINEERING · FEBRUARY 2015

Impact Factor: 0.2 · DOI: 10.1117/12.2086419

4 AUTHORS:

Xiaopeng Peng

Rochester Institute of Technology

4 PUBLICATIONS **4** CITATIONS

SEE PROFILE

Garreth Ruane

Rochester Institute of Technology

10 PUBLICATIONS **9** CITATIONS

SEE PROFILE

Alexandra Artusio-Glimpse

Rochester Institute of Technology

8 PUBLICATIONS **46** CITATIONS

SEE PROFILE

Grover Swartzlander

Rochester Institute of Technology

110 PUBLICATIONS **2,527** CITATIONS

SEE PROFILE

Image Restoration from a Sequence of Random Masks

Xiaopeng Peng, Garreth J. Ruane, Alexandra B. Artusio-Glimpse, and Grover A. Swartzlander, Jr.
Rochester Institute of Technology, Chester F. Carlson Center for Imaging Science,
54 Lomb Memorial Dr, Rochester, NY, USA, 14623

Abstract. We experimentally explored the reconstruction of the image of two point sources using a sequence of random aperture phase masks. The speckled intensity profiles were combined using an improved shift-and-add and multi-frame blind deconvolution to achieve a near diffraction limited image for broadband light (600-670 nm). Using a numerical model we also explored various algorithms in the presence of noise and phase aberration.

Keywords: blind deconvolution, multi-frame, shift-and-add, astronomical imaging.

Address all correspondence to: Xiaopeng Peng, Rochester Institute of Technology, Chester F. Carlson Center for Imaging Science, 54 Lomb Memorial Dr, Rochester, NY, USA, 14623; Tel: +1 585-771-7816; Fax: +1 585-475-5988; E-mail: xxp4248@rit.edu

1 Introduction

High resolution space based telescopes may provide a means to image exo-planets and other astronomical systems. Unlike ground-based telescopes which suffer from the atmospheric turbulence, light pollution, and weather, space-based telescopes are free from these problems and thus provide sharper images. However, modern space-based telescopes have reached a practical cost limit on the size of the effective primary mirror, thereby restricting the achievable resolution in space.

Motivated by Quadrelli's "Granular Mirror Space Telescope[1]" concept , where a cloud of mirrors are randomly distributed along an approximately spherical or parabolic surface, we explored whether computational imaging techniques could be used to extract an image from a random mask that includes piston and tip-tilt phase aberrations. We propose a new framework of multi-frame blind deconvolution to reconstruct a high resolution image from the captured sequence.

2 Related Work

2.1 Shift-and-Add(SAA)

The shift-and-add approach was first introduced[2] for data reduction in speckle imaging. In this technique, each speckle frame is properly shifted and added to an integrated frame. The shift vector is determined so that either the brightest pixel,[3] the centroid of each frame, or the peak of the cross-correlation of two consecutive frames[4] are co-added at the same location, producing a single SAA image[3,4] . The resulting SAA image contains significant diffraction limited component, but sitting on top of a seeing-produced background, which means diffraction limited image can be obtained by simple thresholding[3] or single image deconvolution. SAA has also been demonstrated to be more efficient in tip-tilt correction than adaptive optics control[5,6] .

The simplest form of the SAA method is to shift and add the entire speckle sequence to produce an SAA image with enhanced resolution. However, the single image SAA methods tends to be object dependent, where objects with limited type of shape can be restored. Multi-frame SAA technique[7] overcomes such limitation and results in improved image quality. In this approach,

Computational Imaging XIII, edited by Charles A. Bouman, Ken D. Sauer, Proc. of SPIE-IS&T
Electronic Imaging, SPIE Vol. 9401, 94010D · © 2015 SPIE-IS&T
CCC code: 0277-786X/15/$18 · doi: 10.1117/12.2086419

shift-and-add operations are done in a repetitive way to generate an SAA sequence of speckles, on which multi-frame blind deconvolution is then applied to recover the ideal image.

2.2 Multi-Frame Blind Deconvolution(MBD)

Multi-frame deconvolution recovers target scene from a set of blurry, noisy and distorted observations. Deconvolution algorithms are generally categorized into two types: 1) non-blind deconvolution, where target scene is reconstructed based on complete or partial knowledge of point spread function(PSF) of the imaging system; and 2) blind deconvolution, where target scene and system point spread functions are recovered simultaneously without any additional prior knowledge.

Ayers and Dainty[8] first applied a multi-frame blind deconvolution method to correct for atmospherically degradation. They found object information from a blurry and noisy observation could be recovered without any additional measurement of the distortion. Since the work of Ayers and Dainty, MBD has become an important tool for astronomical image recovery, and has led to a plethora of work, The common approaches are: 1) Batch mode MBD[9] , where all the distorted observations are processed at the same time; 2) Serial mode (or online mode) MBD[10] , where degraded inputs are processed in a streaming way; and 3)Hybrid MBD method, where multiple image recovery algorithms and image enhancement techniques are combined with either batch mode MBD[11] or serial mode MBD[7] .

3 Simulation Methods

3.1 Experimental

A schematic of our experimental system is shown in Fig 1.(a), whereby two quasi-point sources at $d \approx \infty$, subtending an angle θ_0 with respect to the optical axis, are transmitted though a mask placed at the input face of a lens of focal length f = 100mm. An imaging array in the back focal plane (Fourier transform plane) records the speckled images. Using a color filter (not shown) the light sources has a spectral band from 600-670nm. A crumpled cellophane sheet was inserted behind the aperture mask to function as a phase mask. A set of 15 different aperture masks, each having 50 sub-mm sized holes, were prepared by poking a needle through a thin sheet of aluminum foil. A typical speckled image from a single mask is shown in Fig 1.(b). The experimental parameters are summarized in Table 1.(a).

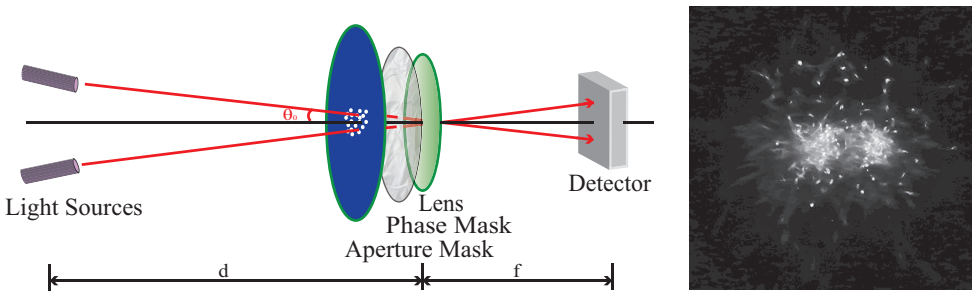

(a) Schematic of laboratory experiment (b) Recorded speckle pattern

Figure 1. Schematic of laboratory experiment and recorded speckle pattern. (a) Schematic of laboratory experiment showing two light sources, masks placed at the input face of a lens, and a focal plane detector array; (b) A typical speckled image in the focal plane owing to a single mask.

3.2 *Numerical*

Following a discussion of our experimental effort, we present a numerical model that affords the ability to control the amplitude and phase mask parameters and establish some bounds for image reconstruction.

3.2.1 *Monochromatic Mutually Incoherent Sources*

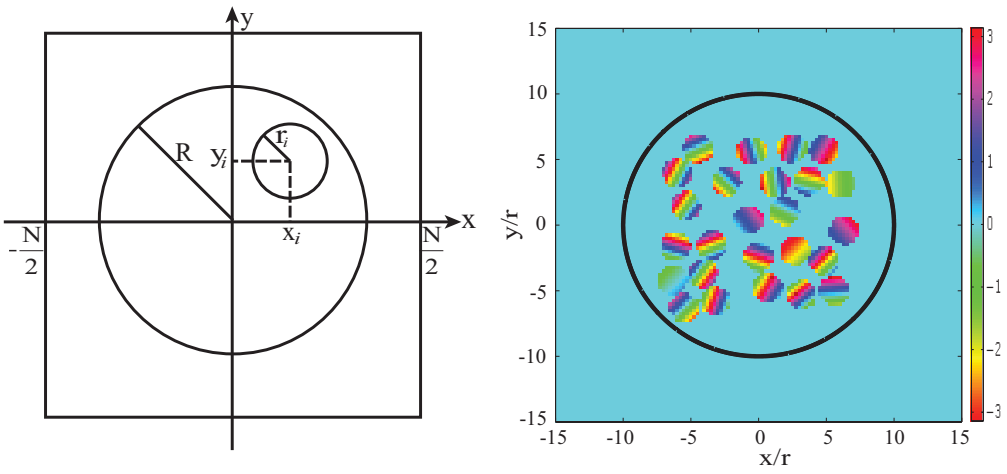

(a) Numerical model of the ramdom mask.

(b) Phase aberrations in sub-apertures. P1=P2=6.

Figure 2. (a) Numerical model depicting a full aperture of radius R, and sub-aperture of radius r_i having a randaom center point (x_i, y_i). (b) False-color phase profile of 25 non-overlapping sub-apertures having random piston and tip-tilt phase.

The numerical model of a random array of small mirrors (or phased apertures) may be represented as a union of non-overlapping sub-apertures of radius r_i that lie within the radius of the full aperture of the telescope R, where the center of each sub-aperture is randomly generated(see Fig 3.(a)). This is represented by the mask function:

$$M(x,y) = [\sum_{i=1}^{n} CIRC(\frac{(x-x_i)^2 + (y-y_i)^2}{r_i^2})]CIRC(\frac{x^2+y^2}{R^2}) \tag{1}$$

where (x_i, y_i) is the center of the i-th sub-aperture, n is the number of subapertures, and $CIRC(z)$ is unity when the argument $z \leq 1$ and zero valued otherwise. To guarantee that sub-apertures are non-overlapping, we impose the condition:

$$\frac{(x-x_i)^2 + (y-y_i)^2}{r_i^2} \cap \frac{(x-x_j)^2 + (y-y_j)^2}{r_j^2} \neq \emptyset, if \quad i \neq j \tag{2}$$

Piston and tip-tilt phase across a given sub-aperture may be represented by the phases:

$$\phi_{pis,i}(x,y) = \pi P_1 rand_1 \tag{3}$$

$$\phi_{tip,i}(x,y) = \pi(x - x_i)P_2 rand_2 \tag{4}$$

$$\phi_{tilt,i}(x,y) = \pi(y - y_i)P_3 rand_3 \tag{5}$$

where P_j is a scaling parameter. To satisfy the Nyquist sampling theorem, we require P_2 and P_3 to be less or equal to unity. A random number generator function $rand_j$ is used for each phase type and each sub-aperture. The system transmission function may be represented by:

$$T(x,y) = \left[\sum_{i=1}^{n} CIRC(\frac{(x-x_i)^2 + (y-y_i)^2}{r_i^2}) e^{i(\phi_{pis,i} + \phi_{tip,i} + \phi_{tilt,i})}\right] CIRC(\frac{x^2+y^2}{R^2}) \tag{6}$$

An example of the phase of this transmission function is shown in Fig 3.(b) for n=25 sub-apertures.

For two point sources at infinity (such as a binary star system) having an apparent angular separation of $2\theta_0$ (see Fig. 1) the electric field from each source, incident upon the telescope, may be expressed as titled plane waves: $exp(ik_x x)$ and $exp(-ik_x x)$, where $k_x \approx 2\pi\theta_0/\lambda$. Furthermore, the electric field in the back focal plane of the system may be expressed as Fourier transforms:

$$E^+(x,y) = FT[T(x,y)e^{+ik_x x}] \tag{7}$$

$$E^-(x,y) = FT[T(x,y)e^{-ik_x x}] \tag{8}$$

where FT is the Fourier transform. Assuming the two light sources are mutually incoherent, we write the intensity in the plane of the detector as:

$$I(x,y) = |E^+(x,y)|^2 + |E^-(x,y)|^2 \tag{9}$$

3.2.2 Polychromatic Mutually Incoherent Sources

To account for a band of wavelengths in the model, we form M different monochromatic waves across a bandwidth, $\Delta\lambda$, each separated by $\delta\lambda = \Delta\lambda/(M-1)$. The intensity in the focal plane may be expressed as the sum of intensities at each wavelength:

$$I_{poly} = \sum_{m=0}^{M} I(\lambda_m) \tag{10}$$

If the intensity profile is known at one wavelength, say λ_0, then by the scaling law of Fourier transforms, the intensity profile at other wavelengths may be quickly found without additional Fourier transform operations. We represent this as:

$$I_i = interp(x_s, y_s, I_0, x_q, y_q) \tag{11}$$

where I_0 is the monochromatic image at the base wavelength λ_0, and I_i, for $i = 1, 2, \cdots, M-1$ is obtained by sampling I_0 at specific sample points, and where $x_s = x\lambda_0 D/N$, $y_s = y\lambda_0 D/N$, and the query points are $x_i = x\lambda_i D/N$, and $y_i = y\lambda_i D/N$, where $D = 2R$ is the diameter of the

telescope, N is the size of the numerical grid (image). Fig 3. shows a typical monochromatic and a polychromatic speckle image.

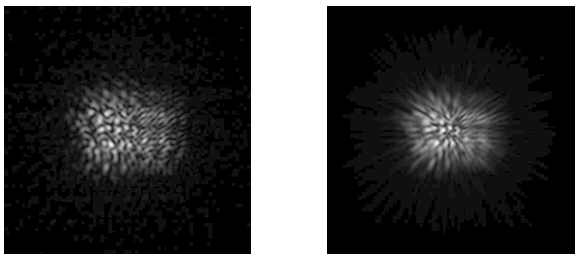

(a) Monochromatic (b) polychromatic

Figure 3. Numerical simulated monochromatic and polychromatic speckle images of the binary star system using a single mask with 25 non-overlapping sub-apertures, each of which has phase aberrations of P1=P2=6. (a) a monochromatic speckle image obtained at a wavelength λ=520nm; (b) a polychromatic speckle images obtained at wavelengths range from 520nm to 670nm, with the wavelength interval of 5nm.

3.2.3 Noise

To get a sense of the effect from noise, in this paper we make a simple inclusion of photon shot noise using the Poisson model. Poisson model assumes that each pixel of an image I(x,y) is affected by noise that follows the Poisson distribution with parameter $\Lambda = I_0(x, y)$, where I_0 is the noise free image:

$$P\{I(x, y) = k\} = \frac{\Lambda^k e^{-\Lambda}}{k} \tag{12}$$

Here we use Matlab build-in function $poissrnd$ to simulate images that affected by photon shot noise:

$$I(x, y) = poissrnd(sI_0(x, y)) \tag{13}$$

where s is a constant that controls the number of photons per pixel. Fig 4. shows three polychromatic speckle images with different photon noises, where s is set to 1/20, 1, and 20 respectively.

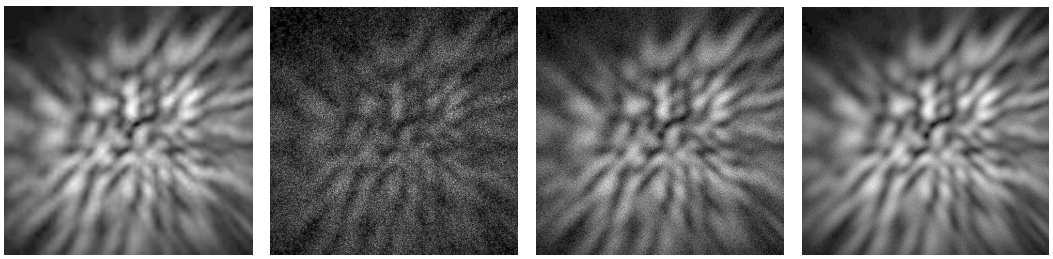

(a) noise free (b) s = 1/20 (c) s=1 (d) s=20

Figure 4. Various levels of shot noise are added to the polychromatic speckle image shown in Fig. 3(b). (a) Noise free speckle image; (b)-(d) speckle images with shot noise generated from increased number of photons per pixel, where s is set to 1/20, 1, and 20 respectively. Only the center portion of the images are shown.

4 Image Reconstruction

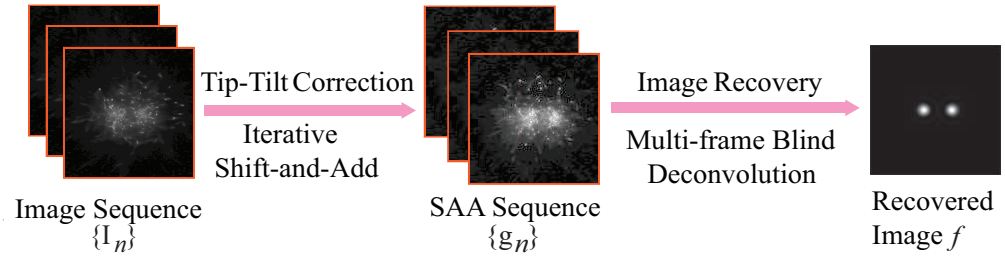

Figure 5. Block diagram of the proposed image reconstruction framework.

In this section, we describe how to use the proposed MBD framework to restore the target image from the recorded speckle patterns. As is shown in Fig 5, the proposed image reconstruction framework contains two major steps:
1. Tip-tilt error is corrected using the proposed iterative multi-frame shift-and-add method. Given the captured speckle sequence $\{g_n\}$, this step corrects phase errors induced by random tip-tilt of each micro-mirror.

2. Image is reconstructed using multi-frame blind deconvolution. In this step, a mutli-frame blind deconvolution[9] is implemented on the obtained SAA sequence $\{SAA_n\}$ to reconstruct a diffraction-limited image f.

4.1 Iterative Shift-and-Add

Here, we implement an improved SAA method based on multi-frame SAA[7] . In Kuwanura[7]'s approach, two consecutive images I_n and I_{n+1} in an image sequence are cross-correlated and the location of the peak of the cross correlation is used as the shifting vector to shift image I_{n+1}. I_{n+1} is then updated by adding I_n and the shifted I_{n+1}. This is repeated until the last image in the sequence is included. This method, however, is highly depend on the order of frames in a sequence. In order to avoid this problem, we repeat iterations multiple times in a circular manner, where the first image is correlated with the last image in the sequence at each iteration as well. We call this method as iterative shift-and-add (ISAA). During the ISAA, all the images in the sequence will be correlated, shifted and integrated in a circular iterative way. By doing this, the dependence of the result on the frame order in a particular sequence can be reduced. In addition, since the iterations are applied to the entire sequence multiple times, random noise is significantly suppressed. Pseudo-code of ISSA method is illustrated in Algorithm 1.

4.2 Multi-frame Blind Deconvolution

Once tip-tilt errors are corrected, a diffraction-limited image f can be restored from the SAA sequence $\{g_n\}$ using the multi-frame blind deconvolution algorithm. Assume that at each time point $n = 1, 2, \cdots, T$, the distorted speckle image is g_n. The image formation process can be modeled as:

$$g_n(\mathbf{x}) = (z \otimes h_n \otimes h)(\mathbf{x}) + q_n(\mathbf{x}) = (f \otimes h_n)(\mathbf{x}) + q_n(\mathbf{x}) \tag{14}$$

Algorithm 1: Iterative Shift-and-Add(ISAA)

Input: Image sequence $\{I_n\}$
Number of iterations and frames: $iter\_num, T$
Output: SAA sequence $\{g_n\}$
for $i = 1; i < iter\_num; i{+}{+}$ **do**
  for $n = 1; n < T; n{+}{+}$ **do**
    if $n == N$ **then**
      $u = I_n$, $v = I_1$
    else
      $u = I_n$, $v = I_{n+1}$
    end
    2D Cross-correlation(CC): u and v
    Peak of CC as shift vector: $(\Delta x, \Delta y)$
    Shift: $v = v(x + \Delta x, y + \Delta y)$
    Integral: $v = u + v$
  end
end
$\{SAA_n\} = \{g_n\}$

Algorithm 2: Alternating Minimization

Input: Image sequence $\{g_n\}$
Output: Restored image f and PSFs $\{h_n\}$
Initialize $f^{(0)}$, $\{h_n\}^{(0)}$ and E^0
$i = 1$
while $E^{(i)} > \frac{|E^{(i)} - E^{(i-1)}|}{|E^{(i)}| + |E^{(i-1)}|}$ **do**
  $\{h_n\}^{(i)} = \arg\min\ E(\{h_n\}^{(i-1)}, f^{(i-1)})$
  $f^{(i)} = \arg\min\ E(\{h_n\}^{(i)}\ ,\ f^{(i-1)})$
  $E^{(i-1)} = E^{(i)}$
  Update $E^{(i)}$ using $\{h_n\}^{(i)}$ and $f^{(i)}$
  $i = i + 1$
end

where $\otimes$ denotes 2D convolution operator. f and q_n represent the diffraction-limited image and random noise in the n_{th} observed image respectively. The vector $\mathbf{x} = (x, y)$ denotes the 2D spatial position in the image. h_n represents the time varying PSF in the n_{th} time frame, due to the temporally changing distribution and piston of the mask. h is the diffraction limited PSF due to system optics, which is invariant of time. We call $f = z \otimes h$ the diffraction-limited image which can be restored using the multi-frame blind deconvolution.

Previously,[12] we have shown that online mode MBD[10] only works for GMST data when prior knowledge of point spread function is available. Here, we implement a batch mode MBD,[9] where the ideal image and PSFs are recovered from the observed images by minimizing the following error metric:

$$Error = E_{\text{conv}} + E_{\text{img}} + E_{\text{bl}}, \tag{15}$$

where E_{conv} is the convolution error term, E_{img} is the image error term, and E_{bl} is the band limited term. Each of these expression are defined below.

The convolution error is given by

$$E_{\text{conv}} = \frac{1}{T^2} \sum_{i=0}^{T} \sum_{\mathbf{u}} \left| \tilde{G}_i - \tilde{F}\tilde{H}_i \right|^2 (\mathbf{u}) B(\mathbf{u}) \tag{16}$$

where $\mathbf{u}$ is the position vector in frequency space and $\tilde{G}_i, \tilde{F}, \tilde{H}_i$ are the Fourier transform of the observed images G_i, ideal image F, and PSFs H_i, respectively. B is a binary mask which is unity for spatial frequencies less than the cut-off frequency and zero elsewhere. By minimizing the convolution term, the difference between each observed image and the convolution of the idea image and each PSF is minimized.

The image term is

$$E_{\text{img}} = \sum_{\mathbf{x}\in\gamma}[F(\mathbf{x})]^2 + \sum_{i=0}^{T}\sum_{\mathbf{x}\in\gamma}[H_i(\mathbf{x})]^2 \tag{17}$$

where γ is the set of pixels in F and $\{H_n\}$ that have negative values. The purpose of the image term is to prevent negative values in both F and $\{H_n\}$ that might be generated in the minimization process.

The band limited term is written

$$E_{\text{bl}} = \frac{1}{T^2}\sum_{i=0}^{T}\sum_{\mathbf{u}}|\tilde{H}_i(\mathbf{u})|^2 B(\mathbf{u}) \tag{18}$$

The purpose of band limit term is to prevent the algorithm from converging to a result where point spread function is zero except for a single pixel.

The overall $Error$ in Eq. 15 is non-convex due to its joint dependence on f and h_n through the convolution operation. However, E is convex with respect to each variable individually with the other held fixed. Therefore, the minimization of E is done in an alternating scheme, as is shown in Algorithm 2. A conjugate gradient method is used to search for the minimum in the error function. The optimum searching step is calculated using backtracking line search[13] .

5 Experiments

Table 1. Parameters in Numerical Simulation and Laboratory Experiment

(a) Parameters of laboratory experiment

Parameter	Value
Diameter of telescope(mm)	~ 6.0
Diameter of sub-aperture(μm)	~ 30
Number of sub-aperture	~ 50
CCD pixel size(μm)	6.25
Wavelength bandwidth(nm)	[600,670]
Exposure time(sec)	0.1
ISO	500
Magnitude ratio of binary stars	1:1

(b) Parameters of numerical simulation

Parameter	Value
Numerical grid size (samples)	2048x2048
Diameter of telescope(samples)	51.1
Radius of sub-aperture(samples)	8
Number of sub-aperture	25
Wavelength bandwidth(nm)	[520,670]
Wavelength sampling interval(nm)	5
Angular separation of binary stars (rad)	3λ/D
Magnitude ratio of binary stars	1:1

We have processed a sequence of experimental speckle data as shown in Fig 6. The sequence, which consists 15 frames of a binary star system, is obtained using the experimental setup described in Section 3.1 and under the conditions listed in Table 1.(a). Figure 7. shows the selected frames of temporal evolution of the proposed MBD framework applied to the experimental sequence, where the last frame represents the final reconstructed image. The spatial separation and the magnitude ratio of the binary stars are accurately calculated.

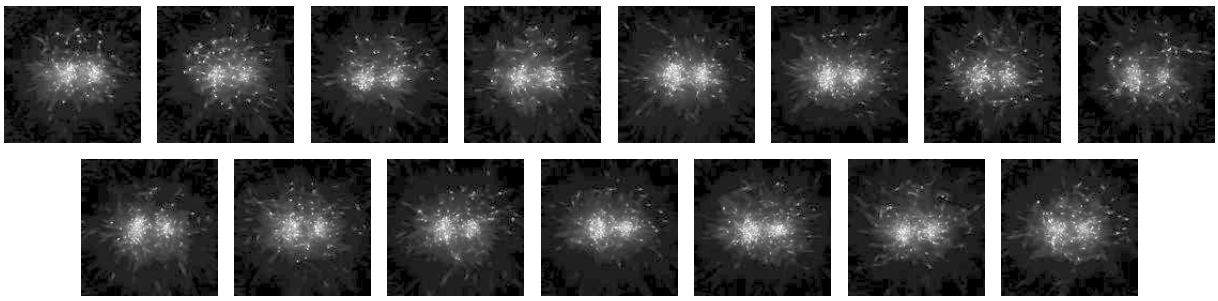

Figure 6. Experimental image sequence consisting of 15 frames. The relevant parameters are listed in Table 1.(a).

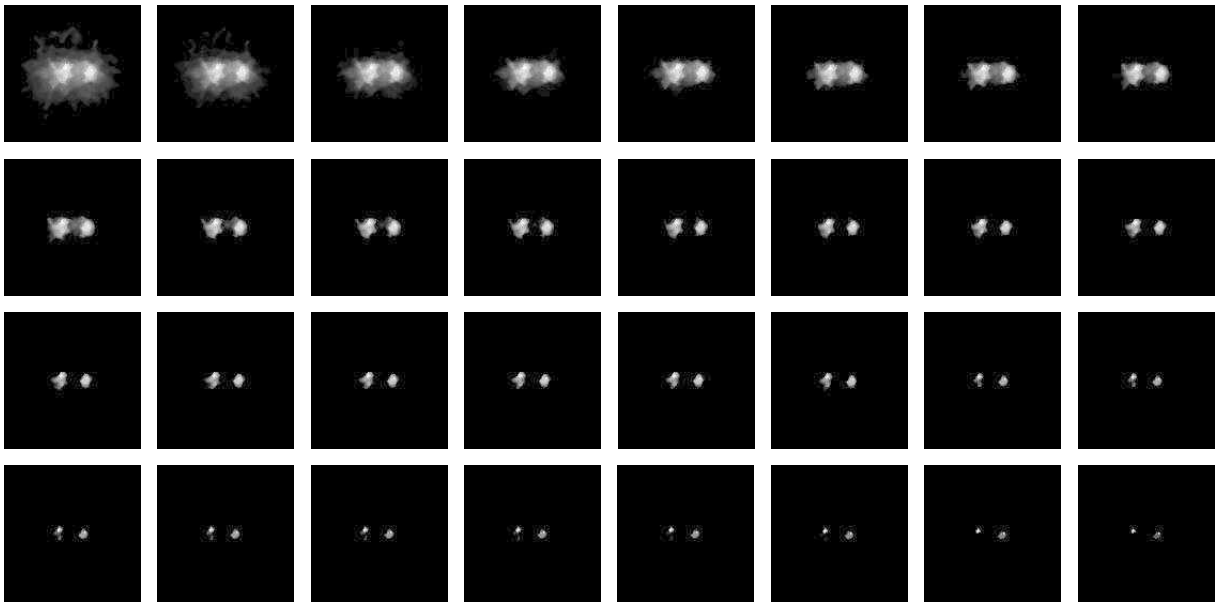

Figure 7. Temporal evolution (selected frames) of the results calculated using our MBD method applied to the experimental image sequence shown in Fig 6.

To further investigate the performance of the proposed MBD, numerically simulated sequences of a binary star system are obtained under conditions listed in Table 1.(b) and with controlled phase aberration, noise level, and angular separation and magnitude ratio of a binary star system. A ground truth image of the binary stars is also simulated numerically for verification. We compare our results against two alternative methods[7,9] , and show that our method yields improved results in recovering the simulated speckle images. We also demonstrate the robustness of our method to large piston errors, tip-tilt errors, and noise level.

We evaluate the algorithm performance quantitatively using three metrics: the spatial separation error, the magnitude ratio error, and the reconstruction error. The spatial separation error is given by

$$E_{\text{sep}} = \frac{|d_0 - d|}{d_0}, \tag{19}$$

where d_0 and d are the true and calculated distances between the peaks of the binary stars, respectively. This metric indicates the accuracy of the locations of recovered binary stars. The magnitude

ratio error is

$$E_{\text{mag}} = \frac{|m_0 - m|}{m_0} \tag{20}$$

where m_0 and m_0 are the true and calculated peak-to-peak magnitude ratios of the stars, respectively. This error metric reflects the accuracy of the recovered intensities of the binary star system. Lastly, the reconstruction error is written as:

$$E_{\text{rec}} = \sum_{i=0}^{T} \sum_{\mathbf{x}} |g_i - f \otimes h_i|^2(\mathbf{x}), \tag{21}$$

where f is the reconstructed image, h_i is the i_{th} reconstructed PSF, and g_i is the i_{th} captured image in the sequence. This error metric compares the reconstructed image to the ideal image.

In addition, to quantify the amount of noise in each sequence, we define signal-to-noise ratio (SNR) of a single frame as the power ratio between a signal and the noise:

$$SNR_n = \frac{P_{f_n}}{P_{q_n}} \tag{22}$$

where f_n is the n_{th} frame in a noise contaminated speckle sequence, q_n is the photon noise affects f_n, P is the average power. We then average over the computed SNR of each frame as the SNR of the noise affected sequence:

$$SNR = \frac{1}{T} \sum_{n=1}^{T} SNR_n \tag{23}$$

We apply the proposed MBD framework, Jefferies[9] MBD, and Kuwamura[7] MBD to a numerically simulated noise free image sequence assuming P1=1,P2=1 (see Figs 8.). The proposed MBD yields the best results. In addition, the separation error of reconstructed binary stars using the proposed MBD is less than 0.1% and the magnitude ratio error is less than 2% (see Table 2).

We demonstrate the influence of the phase aberration on the reconstruction results by applying the proposed MBD to the speckle sequences with different piston and tip-tilt errors. The results are shown in Fig. 9 along with the ground truth image. The associated quantitative errors are shown in Table 2. The proposed MBD accurately recovers the image with low error of spatial separation and magnitude ratio of binary star system. However, as the piston and tip-tilt error increase to P1 = P2 = 6, the image of the stars is displaced and rotated relative to the stars in ground truth image although their spatial separation and magnitude ratio are still accurately calculated.

Noise can also strongly affect the performance of the image reconstruction. We examine the influence of noise level on the performance of the proposed MBD by adding different amount of photon noise to the simulated image sequence. We compare the restoration results from noise free and noisy sequence with the ground truth image in Fig 10, and show associated quantitative errors in Table 3. As expected, the accuracy of reconstruction suffer with decreasing SNR. Particularly, the magnitude ratio accuracy is more sensitive to noise than the spatial separation.

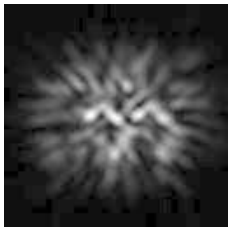

(a) P1=1, P2=1

(b) Proposed MBD (c) Jefferies[9] MBD (d) Kuwamura[7] MBD (e) Ground Truth

Figure 8. Reconstruction results of the proposed MBD, Jefferies[9] , and Kuwamura[7] methods applied to a numerical simulated noise free speckle sequences of binary star system with P1=1,P2=1. (a) A typical frame of the binary star system from the speckle sequence; (b)-(d) Reconstruction results using different methods, where only the proposed MBD produces acceptable result;(d) Ground truth image of the binary star system.

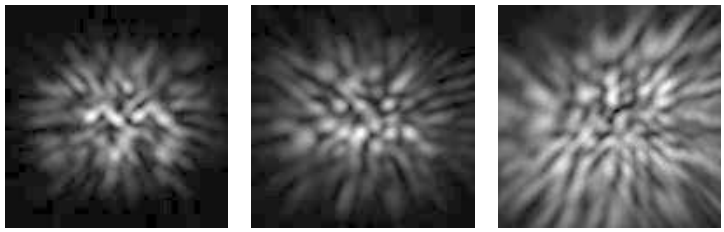

(a) P1=1, P2=1 (b) P1=3, P2=3 (c) P1=6, P2=6

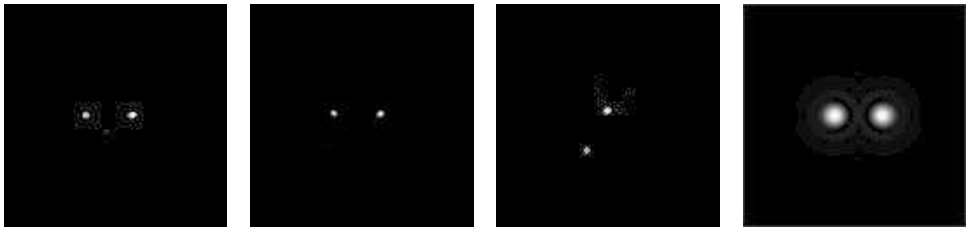

(d) P1=1, P2=1 (e) P1=3, P2=3 (f) P1=6, P2=6 (g) Ground Truth

Figure 9. Reconstruction results of the proposed MBD method applied to three numerical simulated speckle sequences with different phase aberration level. (a)-(c) A typical frame from each speckle sequence; (d)-(f) Corresponding reconstruction results; (f) As the phase aberration increases, the algorithm may fail to reconstruct an accurate image; (g) Ground truth image.

.

	E_{sep}	E_{mag}	E_{rec}
P1=P2=1	0.0005	0.0196	0.0118
P1=P2=3	0.0243	0.2687	0.0125
P1=P2=6	0.0573	0.3821	0.0181

Table 2. Errors of reconstructed results using proposed MBD applied to speckle sequences with different phase aberrations. The reconstruction errors increase with phase errors.

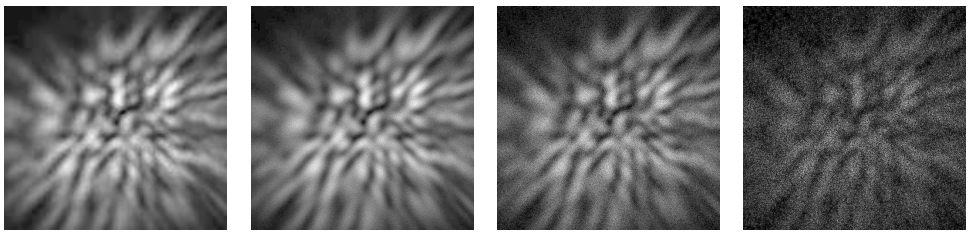

(a) Noise free (b) SNR = 2.6075 (c) SNR = 0.2067 (d) SNR = 0.0481

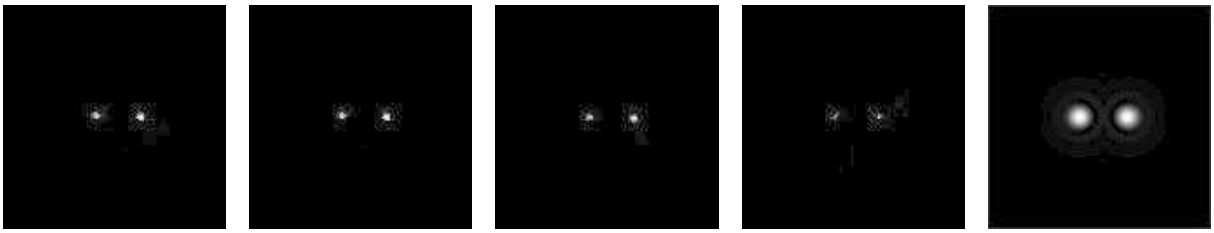

(e) Noise free (f) SNR = 2.6075 (g) SNR = 0.2067 (h) SNR = 0.0481 (i) Ground Truth

Figure 10. Reconstruction results of the proposed MBD method applied to numerical simulated speckle sequences with various SNR and P1=P2=6. (a) A noise free frame; (b)-(d) A typical frame from each noisy speckle sequence; (e)-(h) Corresponding reconstruction results. (i) The ground truth image. The results are processed so that the object coordinate of recovered binary stars is in accordance with the world coordinate for display purposes.

	E_{sep}	E_{mag}	E_{rec}
Noise free	0.0573	0.3821	0.0181
SNR = 2.6075	0.0591	0.4011	0.0213
SNR = 0.2067	0.0823	0.7786	0.0256
SNR = 0.0481	0.0908	0.9833	0.0384

Table 3. Errors of reconstructed results of proposed MBD applied to speckle sequences with varying SNR.

6 Conclusion

In this paper, we explored an imaging reconstruction technique that may be applicable to random aperture imagers such as a "Granular Mirror Space Telescope[1]". We experimentally and numerically demonstrate that a multi-frame blind deconvolution technique can recover a diffraction-limited image from a random sequence of recorded patterns. The restoration results of the proposed

MBD framework outperformed a few existing MBD methods, and is robust to phase aberration and noise, although increased phase errors and decreased SNR were found to lead to a minor decline of the performance of the proposed MBD, that is, the error in measured spatial separation, magnitude ratio of the binary stars in the reconstructed image is increased. These results provide a promising path toward a new imaging system based on a randomly varying array of sub-apertures or small reflectors.

7 Acknowledgments

We are grateful for discussions about granular telescopes with Marco Quadrelli and Scott Basinger, Jet Propulsion Laboratory, Pasadena, CA. This work was funded by the US National Science Foundation (ECCS-1309517) and by a NASA NIAC Phase I (Jet Propulsion Laboratory) contract.

References

1 M. B. Quadrelli, S. Basinger, and G. A. Swartzlander, "Orbiting rainbows: Optical manipulation of aerosols and the beginnings of future space construction." `http://www.nasa.gov/sites/default/files/files/Quadrelli_2012_PhI_OrbitingRainbows_.pdf`. Accessed June 18, 2013.

2 R. Bates and F. Cady, "Towards true imaging by wideband speckle interferometry," *Optics Communications* **32**(3), 365–369 (1980).

3 C. Lynds, S. Worden, and J. W. Harvey, "Digital image reconstruction applied to alpha orionis," *The Astrophysical Journal* **207**, 174–180 (1976).

4 N. Baba, S. Isobe, Y. Norimoto, and M. Noguchi, "Stellar speckle image reconstruction by the shift-and-add method," *Applied optics* **24**, 1403–1405 (1985).

5 J. C. Christou, "Image quality, tip-tilt correction, and shift-and-add infrared imaging," *Publications of the Astronomical Society of the Pacific* , 1040–1048 (1991).

6 V. Orlov and V. Voitsekhovich, "Analysis of chromatic effects in the shift-and-add method," *Revista mexicana de astronomía y astrofísica* **44**(2), 325–329 (2008).

7 S. Kuwamura, Y. Azuma, N. Miura, F. Tsumuraya, M. Sakamoto, and N. Baba, "Multiframe blind deconvolution applied to diverse shift-and-add images of an astronomical object," *Optical Review* **21**(1), 9–16 (2014).

8 G. Ayers and J. C. Dainty, "Iterative blind deconvolution method and its applications," *Optics letters* **13**(7), 547–549 (1988).

9 S. M. Jefferies and J. C. Christou, "Restoration of astronomical images by iterative blind deconvolution," *The Astrophysical Journal* **415**, 862 (1993).

10 S. Harmeling, M. Hirsch, S. Sra, and B. Scholkopf, "Online blind deconvolution for astronomical imaging," in *Computational Photography (ICCP), 2009 IEEE International Conference on*, 1–7, IEEE (2009).

11 M. Hirsch, S. Harmeling, S. Sra, and B. Schölkopf, "Online multi-frame blind deconvolution with super-resolution and saturation correction," *Astronomy and Astrophysics-Les Ulis* **531**, 1217 (2011).

12 X. Peng and G. A. Swartzlander, "Mirror swarm space telescope," in *Image and Signal Processing Workshop (WNYISPW), 2014 IEEE Western New York*, 37–41, IEEE (2014).

13 L. Armijo, "Minimization of functions having lipschitz continuous first partial derivatives," *Pacific Journal of mathematics* **16**(1), 1–3 (1966).